Theory and Practice of Science and Technology
2025, VOL. 6, NO. 3, 165-174
DOI: 10.47297/taposatWSP2633-456932.20250603

CFD simulation study on the effect of multiple interceptor-enhanced structure on flash vaporization characteristics

Wanqiong Bao, Zhishan Bai

School of Mechanical and Power Engineering, East China University of Science and Technology

ABSTRACT

As a special process in evaporation and concentration technique, flash evaporation is widely used in seawater desalination, low-temperature waste heat utilization and other fields. Traditional flash evaporation process exists its own problems such as high energy consumption, long process and complicated equipment. For this reason, it is of great significance to develop a new type of reinforced internal components. The research methodology of this paper is numerical simulation. Under different structural parameters of the reinforced internal component, a three-dimensional computational model for the flash evaporation process is developed in this paper. Also, the influence of the new reinforced internal component on the flashing characteristics will be explored. Specifically, with emphasis on the change of the flash evaporation process under different top angles θ, number of layers N, and aperture ratios E. The Results show that when the top angle θ increasing, the falling speed of the incompletely flashed liquid on the structure face is slowed down. The flash evaporation rate at θ=150° is greater than that at θ=90°. Its growth rate is 81.91%. With the increase of the number of layers N, the liquid's retention time in the flashing environment is extended, which facilitates the completion of the entire flashing process. The flash evaporation rate is also enhanced at N=5 compared with that at N=2. Its growth rate is 17.51%. At last, with the increase in the aperture ratios E, the growth rate of flash evaporation rate reaches up to 100.84% between E=3/46 and E=3/184.

KEYWORDS

Process intensification; Negative-pressure flash evaporation; Numerical simulation; Multiple intercepting internal component

1 Introduction

Flash evaporation is a special process in evaporation and concentration technique, The process refers to the liquid at a certain temperature entering an environment below the saturation pressure corresponding to the certain temperature, due to the sudden reduction in pressure, the liquid is unable to store its apparent heat. So, the heat is released in the form of sensible heat., which causes the liquid to be rapidly vaporized. Concomitantly, this is a violent phase change evaporation phenomenon [1]. It is because of its outstanding performance characteristics such as fast heat transfer, high separation efficiency, good cooling effect and high steam generation compared with other evaporation and concentration techniques, flash evaporation is widely used in the fields of seawater desalination [2-3], low-grade energy utilization [4], reduction of harmful emissions from power plants [5], marine steam accumulator [6], drug drying [7], and ocean thermal energy conversion [8-9]. Nevertheless, the traditional flash evaporation process is still subject to numerous limitations, which give rise to several problems. These include high energy consumption, a lengthy process and the necessity for complex equipment.

However, the theoretical approach to process intensification can provide solutions to the above problems. Process intensification is an approach aimed at improving process efficiency and effectiveness [10]. The fundamental principle of chemical process intensification is the exploitation of the transfer, reaction and equilibrium characteristics of a chemical process across diverse systems. This is achieved through the utilization of innovative equipment and technology, which enhances the rate of the process. Consequently, the process is completed in a shorter time, with an increased conversion rate of the product, a reduction in the size of the equipment employed and a decrease in the quantity of material required for production [11-12]. In the current published literature and existing industrial cases, many process intensification methods be used in evaporation fields, such as ultrasonic field intensification, supergravity field intensification, microwave field intensification, and novel tower structure intensification, etc. [13]. Therefore, optimizing flash evaporation technique by using process enhancement theory methods can improve energy efficiency, reduce process complexity, and lower industrial production costs. At the same time, it is more conducive to sustainable development in the production of evaporation and concentration processes.

Throughout the flash evaporation process is mostly carried out inside the closed tank, it is difficult to observe its occurrence in real time, and it is difficult to monitor the internal fluid state, so numerical simulation is an important means of analyzing and predicting the flash evaporation process [14]. The current numerical simulations for the process enhancement aspect mainly focus on the structural optimization of desalination flash chamber. Pang Hong[15] et al. used numerical simulation to calculate and analyze the flow field inside the flash chamber from the perspective of hydrodynamics, to explore ways to improve the efficiency of the desalination plant. The result show that through the reasonable arrangement of the flow stopper structure in the flash chamber, the reflux can be improved and the flow energy loss can be reduced. Furthermore, the flow stopper structure can make the upper and lower fluid layers form a strong reflux, to improve the efficiency of flash evaporation. Yao Zheng[16] et al. calculated the secondary desalination flash chamber by CFD numerical simulation method, and analyzed the streamline spectral pattern of vortex and turbulent viscosity of the fluid flow field with and without flow stopper, and optimized the structural arrangement of the bottom of the flash chamber. Qi Chunhua[17] and others used Fluent software to simulate and analyze the flow state, gas-liquid phase content distribution, velocity field and temperature field in the flash chamber of low-temperature multi-effect seawater desalination, and proposed an optimal design scheme for the diameter of the flash tank, the length of the tank body, and the height of the internal platform on the basis of the analysis results. Cao Tianyi[18] et al. analyzed the fluid flow state inside the flash chamber with additional porous plates at the bottom by numerical simulation, and investigated the effects of parameters such as Reynolds number, number of orifices and equivalent aperture ratio on the pressure loss of seawater in the process of seawater flow, and the results showed that the increase of the number of orifices and the equivalent aperture ratio is conducive to the reduction of the pressure loss.

The results of the above studies provide fundamental guidance for this paper in terms of numerical simulation, indicating the influencing factors and analytical methods that need to be considered. However, the research at present on the combination of flash evaporation technology and process strengthening theory is still in the development stage, and few scholars have designed new internal components for the flash evaporation process. Therefore, based on the vacuum flash evaporation process and the theoretical method of process intensification, this paper proposes a flash evaporation chamber with multiple intercepting and intensifying internal component, and carries out the simulation and analysis by numerical simulation. Particularly, focusing on the effects of different internal component parameters and dimensionless number variations on flash characteristics and internal flow field. It is hoped that this will provide guidance for the future design of this device.

2 Mathematical modelling

The flash evaporation process belongs to the gas-liquid two-phase flow problem in multiphase flow in Computational Fluid Dynamics. Currently, there are two main methods for numerical simulation and calculation of multiphase flow in Fluent: Euler-Lagrange approach [19] and Euler-Euler approach [20]. In this paper, the mixture model in the Eulerian-Eulerian method is used to describe the vapor-liquid two-phase flow in the flash evaporation process. The vaporization condensation model is used to describe the heat and mass transfer in the process. The Realizable k-ε model is used to calculate the turbulent flow. Among them, the specific forms of the mixed multiphase flow model and the evaporation condensation model are shown below:

2.1 Mixture multiphase model

Mixture model have excellent performance in solving complex multiphase flow problems and can simulate the interaction between fluids with different properties and characteristics. Its formulation can be divided into two parts, which are the mass transfer equation and the Navier-Stokes equation [21].

The mass transfer equation:

$$\frac{\partial(\rho_i \alpha_i)}{\partial t} + \nabla \cdot (\rho_i \alpha_i u) = \nabla \cdot (\Gamma_i \nabla \alpha_i) + S_i \tag{1}$$

where ρ_i represents the density of the i-th substance, α_i represents the volume fraction of the i-th substance, u represents the velocity of the fluid, Γ_i represents the diffusion coefficient of the i-th substance, and S_i represents the source term, e.g. a substance resulting from a chemical reaction.

Navier-Stokes equation:

$$\frac{\partial(\rho u)}{\partial t} + \nabla \cdot (\mu(\nabla u + \nabla u^T)) + \nabla p = \sum_{i=1}^{N} \nabla \cdot ((\mu + \mu_t^i)(\nabla u^i + (\nabla u^i)^T)\alpha) + \rho g \tag{2}$$

where ρ represents the density of the fluid, u represents the velocity of the fluid, p represents the pressure of the fluid, μ and μ_t^i respectively represents the dynamic viscosity of the fluid and the dynamic viscosity of the i-th substance, and g is the acceleration of gravity. The equation describes the laws of motion and interaction of fluids in a complex multiphase environment.

2.2 Vaporization-condensation model

The vapor phase mass transfer equation describes the interphase mass transfer mechanism between the liquid and vapor phases [22].

$$\frac{\partial}{\partial t}(\alpha_v \rho_v) + \nabla \cdot (\alpha_v \rho_v \vec{V}_v) = \dot{m}_{lv} - \dot{m}_{vl} \tag{3}$$

where subscript α_v = vapor volume fraction, ρ_v = vapor density, $\vec{V}_v$ = vapor phase velocity vector, $\dot{m}_{lv}$ = mass transfer rate from liquid to vapor phase, and $\dot{m}_{vl}$ = mass transfer rate from vapor to liquid phase.

If $T_l > T_{sa}$ (vapourisation), then

$$\dot{m}_{lv} = corff \cdot \alpha_l \rho_l \frac{(T_l - T_{sat})}{T_{sat}} \tag{4}$$

If $T_v > T_{sa}$ (condensation), then

$$\dot{m}_{lv} = corff \cdot \alpha_l \rho_l \frac{(T_l - T_{sat})}{T_{sat}} \tag{5}$$

where subscript α_l = liquid volume fraction, ρ_l = liquid density, T_l = liquid phase temperature, T_v = vapor phase temperature, and T_{sat} = saturation temperature.

3 Computational case setup

The flash chamber is modeled by SolidWorks software. Fig. 1(a) shows the three-dimensional model. The flash tank has a 240mm height, a 100mm internal diameter and a 10mm wall thickness and contains multiple interceptor-enhanced internal components. Fig. 1(b) is the schematic diagram of the multiple interceptor-enhanced internal components. The whole shape of the inner member is a multi-layer umbrella-plate type structure, the outer diameter is 92mm, the total height is 186mm, the interval of the umbrella-plate structure is 35mm. θ is the top angle of the inner structure, N is the number of layers, and d is the diameter of the hole in the umbrella-plate structure.

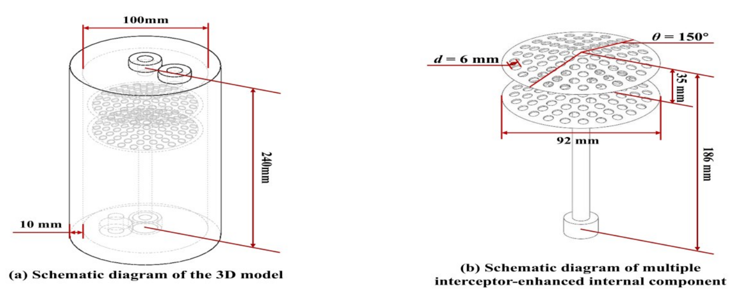

Figure 1 Schematic Structure of Multiple Interceptor-enhanced

On one hand, the internal component can increase the time that the liquid stays in the chamber, in order to improve the completion of the flash evaporation; on the other hand, the umbrella-plate wall surface and the holes in the surface can make the liquid convert to different flow states, such as liquid film, droplet and column flow, and this can increase the surface area of the liquid contacting with the flash evaporation environment, so as to achieve the purpose of reinforcing the flash evaporation process.

4 Mesh division and boundary conditions

Considering the physical model and the computational complexity of this paper, a structured hexahedral mesh is chosen to subdivide the model, which greatly improves the computational speed while ensuring accuracy. Fig. 2(a) is shown the situation of grid demarcation.

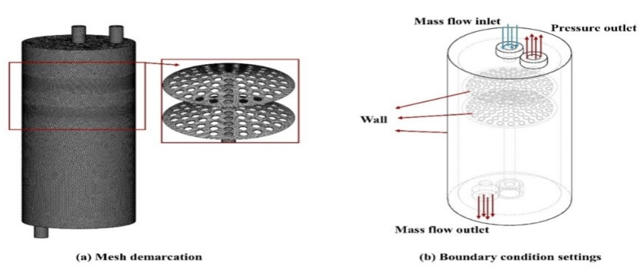

Figure 2 Meshing and Boundary Condition Settings

In order to guarantee the precision of the numerical simulation outcomes and the calculation time, the models are validated for grid-independence. The models are categorized according to their grid densities, resulting in six distinct sets of models with varying grid numbers. These grid numbers are 534390, 706989, 996955, 1171224, 1336633, and 1687093, respectively. The results are shown in Fig. 3. The results indicate that the rate of change in the computational results gradually diminishes as the degree of grid refinement increases. The relative deviation of the outlet steam mass flow rate calculated from the models with grid numbers 1171224 and 1687093 is 0.033%, while the relative deviation of the vacuum pressure in the chamber is 0.09%. Upon reaching a grid count of 1171224, the influence of the grid count on the calculation results is minimal. Furthermore, as the grid count increases, the calculation time also rises. Consequently, the model with a grid count of 1171224 is selected for numerical calculation. Thereafter, models with different umbrella plate structures adopt this meshing method.

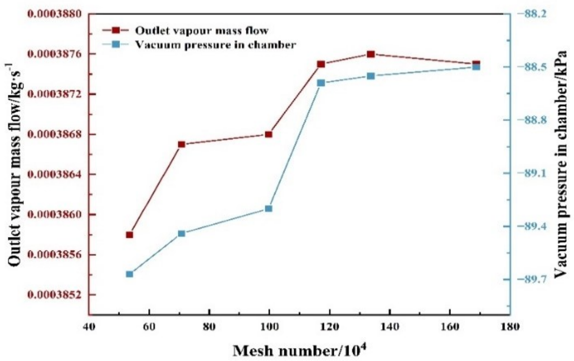

Figure 3 Mesh-independent verification

The boundary conditions are defined in accordance with the established computational domain, which encompasses the liquid inlet, vapor outlet, and wall. The specific conditions are set as illustrated in Fig. 2(b). The liquid inlet is set as mass-flow inlet, the generated vapor outlet is set as pressure-outlet, the liquid outlet is set as mass-flow outlet, the outer wall is set as no-slip wall, and the inner umbrella-plate structure is also set as no-slip wall. In terms of heat transfer, the walls were adiabatic. The cavity and vapor outlet pressures were set to -92 kPa, the inlet mass flow rate to 0.007 kg/s, and the inlet temperature to 80°C.

5 Results

5.1 Evaluation parameters

The flash evaporation efficiency, which represents a crucial indicator of the flash evaporation process, can be calculated using the following formula [23-24]:

$$\eta = \frac{m_{cs}}{m_v} \times 100\% \tag{6}$$

where subscript m_{cs} = mass flow rate of saturated vapor, kg/s, m_v = the inlet mass flow rate, kg/s.

In order to facilitate further analysis of the evaporation and flash evaporation rates obtained experimentally for different operating conditions, the growth rate $\Delta\eta$ is defined to illustrate the enhancement effect of the change in process conditions on the flash evaporation process. The defining equation is shown below.

$$\Delta\eta = \frac{\eta_i - \eta_j}{\eta_j} \times 100\% \tag{7}$$

where i and j are representing experiments under different working conditions.

5.2 Influence of structural parameters on flash vaporization characteristics

5.2.1 Internal component top angle θ

The effects of flash evaporation and flow field characteristics were investigated under the following conditions: number of layers $N = 2$, aperture ratios $E = 3/46$ and top angle $\theta = 90° \sim 150°$. Fig. 4 shows the values of outlet steam mass flow rate and the flash rate obtained from the simulation. The bar graphs and curves in the figure demonstrate that when only the top angle θ is altered, both the outlet steam mass flow rate and the flash evaporation rate increase in proportion to the increase in the top angle θ. Calculated by Equation 7, it can be seen that the flash evaporation rate at θ=150° is enhanced by 81.91% compared with that at θ=90°, which has a sharp improvement.

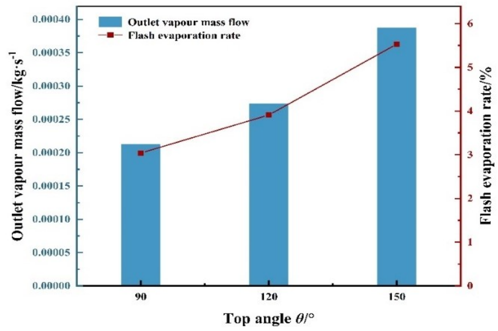

Figure 4 Outlet vapor mass flow and flash evaporation rate at different top angle θ

As illustrated in Fig. 5, when the top angle θ is minimal, the velocity on the multiple intercepting and reinforcing internal component is elevated. This phenomenon indicates that the liquid phase may remain on the umbrella-plate structure for a limited period of time, which may result in a reduction in the strengthening effect. When θ = 90°, the velocity on the surface of first layer of umbrella-plate structure is greater than 5.2 m/s, and the velocity on the surface of second layers of umbrella-plate structure is greater than 3.6 m/s; When θ = 120°, the velocity on the surface of first layer is greater than 4.4 m/s, the velocity on the surface of second layers is higher than 2.8 m/s; When θ = 150°, the velocity on the surface of first layer is higher than 3.6 m/s, and the velocity on the surface of second layers is higher than 1.6 m/s. It has been demonstrated that the velocity of the liquid phase on the surface of the umbrella-plate structure is significantly reduced. The velocity cloud diagram reveals the presence of a pronounced reflux formation in the upper region of the umbrella-plate structure. This phenomenon facilitates the transfer of heat and mass between the vapor and liquid phases within the chamber.

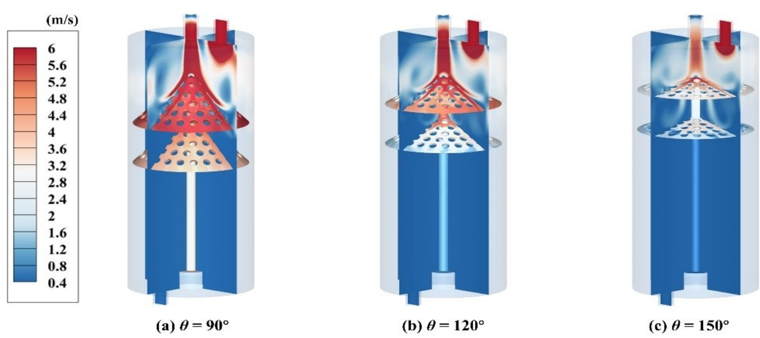

Figure 5 Velocity cloud maps at different top angle θ

Fig. 6 shows the cloud diagram of the vapor phase fraction. Due to the negative pressure conditions present within the chamber, the liquid phase will be rapidly converted to the vapor phase upon entry, with the vapor phase fractions above the first umbrella-plate structure exhibiting a greater than 0.92 concentration. Observing the fraction of the vapor phase between the first and the second umbrella plate structure, there is no obvious phenomenon of generating the vapor phase when θ = 90 °, which indicates that the liquid phase slides to the bottom in the first layer of the umbrella-plate structure more often; When θ =120° and θ =150°, there is an evident phenomenon of vapor phase generation in the region, with a more pronounced effect observed at θ = 150°. This indicates that a greater quantity of incompletely flashed liquid phase can continue the flashing process after it has been well dispersed. Once dispersed, it can continue the flash evaporation process, which improves the completion of flash evaporation.

Fig. 7 illustrates the mean vacuum pressure within the chamber, which is observed to be lower when θ = 150°. This is indicative of a more favorable environment for the flash evaporation process. A lower vacuum pressure corresponds to a lower boiling point, which is conducive to providing more superheat. This, in turn, can reduce the minimum bubble size which can become a vapor core, lower the conditions of vapor nucleation, and increase the number of vapor cores produced. Furthermore, in the stage of bubble growth, the increase in superheat can promote the vaporization process on the vapor-liquid demarcation surface, which can enhance the growth rate of the bubbles. Consequently, the expansion of the number of vapor cores and the acceleration of vapor bubble growth diminishes the particle size of the droplets produced by flash evaporation, enhance the impact of flash atomization, and facilitate the flash evaporation process.

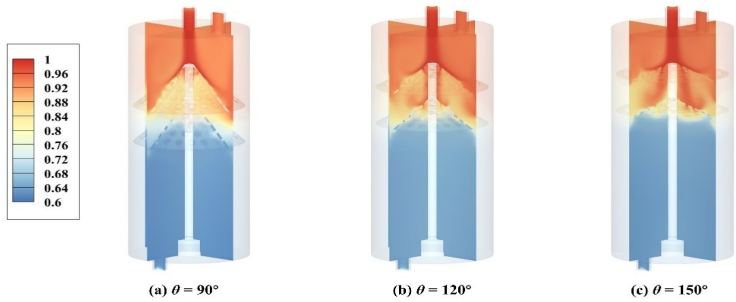

Figure 6 Cloud map of vapor phase fractions at different top angles θ

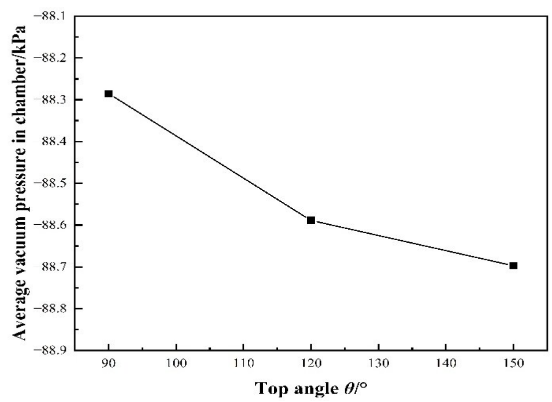

Figure 7 Average vacuum pressure in the chamber at different top angle θ

5.2.2 Number of internal components' layers *N*

The effects of flash evaporation and flow field characteristics were investigated under the following conditions: top angle $\theta = 150°$, aperture ratios $E = 3/46$, and number of layers $N = 2 \sim 5$. From the histograms and curves in Fig. 8, it can be seen that the outlet vapor mass flow rate and the flash evaporation rate improved with the increase in the number of layers N, under the condition that only N got changed. Calculation from Equation 7 shows that the growth rate between $N = 5$ and $N = 2$ is 17.51%.

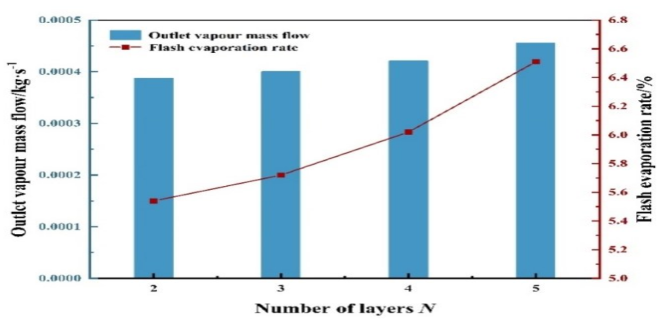

Figure 8 Outlet vapor mass flow rate and flash evaporation rate for different number of internal components' layers N

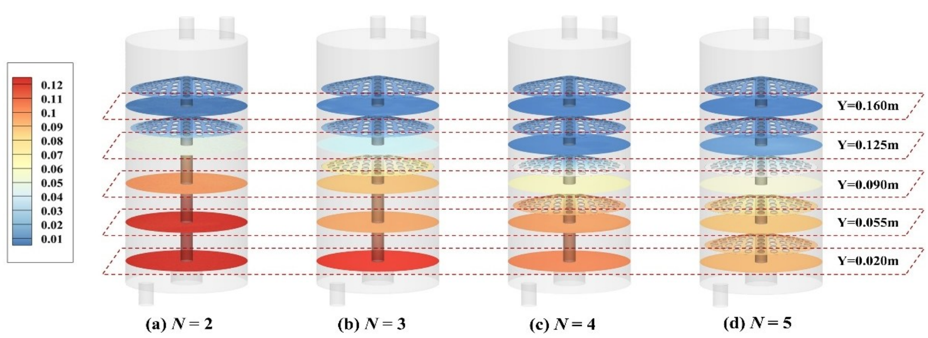

Figure 9 Cloud maps of liquid phase fractions in chamber for different number of internal components' layers N

As can be seen in Fig. 9, the percentage of the liquid phase fraction at different points in the chamber decreases as N increasing. In the cross-section of Y = 0.02 m, when N = 2, the liquid phase fraction is higher than 0.12; when N = 5, and lower than 0.09. This is due to the fact that it exists two type of flash evaporation in the chamber after the liquid enters the flash chamber. One is the flash evaporation of the liquid in the vapor space, and another one is the flash evaporation of the liquid after dropping down to the water space. As the number of layers increases, the liquid phase that is not completely flashed is intercepted layer by layer by the umbrella-plate structure. This can slow its falling rate, add the residence time of the liquid phase in the vapor space, and increase the degree of completion of the flashing process.

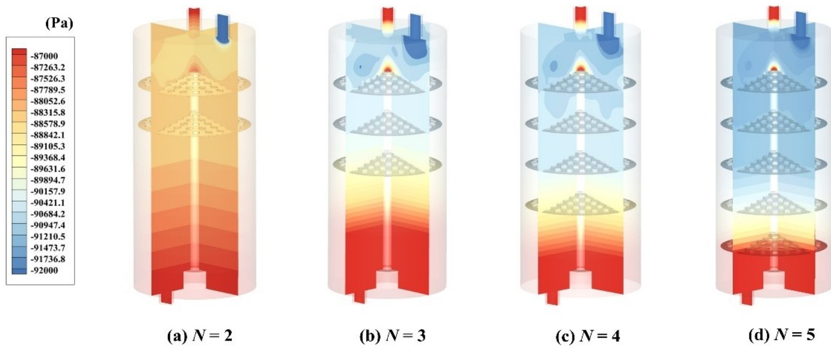

Figure 10 Cloud maps of pressure distribution in chamber for different number of internal components' layers N

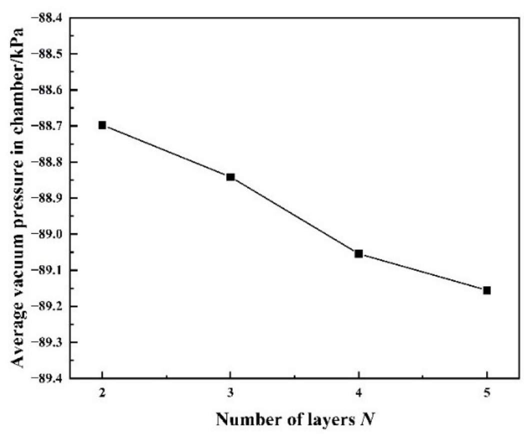

Figure 11 Average vacuum pressure in chamber for different number of internal components' layers N

As can be seen from Fig. 10 and Fig. 11, the vacuum pressure inside the chamber gradually increases when N decreases. This change leads to an increase in the boiling point of the liquid in the corresponding environment. Still, this is not conducive to liquid fragmentation, weakens the flash atomization effect, increases the particle size of the resulting droplets and increases the difficulty of carrying out the flash evaporation process, so higher vacuum pressures are not conducive to the flash evaporation process. In summary, an appropriate increase in the number of multiple intercepting and reinforcing internal components′ layers in the chamber is beneficial to the overall flash evaporation process.

5.2.3 Aperture ratio *E*

The apertures d is the diameter of holes in the surface of the internal umbrella-plate structure component. The apertures d influences whether the liquid entering the chamber can form flow columns and drops and flow smoothly through the aperture to the next layer. If the aperture d is too small, the liquid will not be able to pass through the first layer of the umbrella plate structure due to the tension, and form a pile up on the plate, which will affect the completion of the whole flash evaporation process. In order to more intuitively describe the parameter of aperture d, a dimensionless number aperture ratio $E = d / D$. The aperture ratio E is redefined to express the effect of a change in aperture d by the ratio of aperture d to the diameter of the umbrella-plate structure D. A larger E represents a larger d.

The effects of flash evaporation and flow field characteristics were investigated under the following conditions: number of layers N = 2, top angle θ = 150°, aperture ratios E = 3/184 ~ 3/46. The results presented in Fig. 12 demonstrate that the flash evaporation rate of the multiple interception-enhanced flash evaporation process exhibits an increasing trend as the aperture ratio E is increased gradually. The flash evaporation rate′s growth rate was calculated using Equation 7, which revealed that the flash evaporation at E = 3/46 is enhanced by 100.84% compared with that at E = 3/

184. Furthermore, the growth rate is more than 100%, indicating that *E* has a significant influence on the completion of the flash evaporation process.

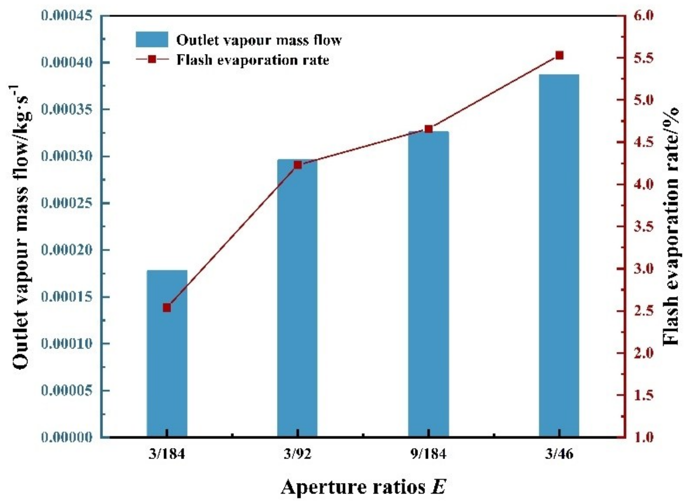

Figure 12 Outlet vapor mass flow rate and flash evaporation rate at different aperture ratios *E*

As illustrated in Fig. 13, when *E* is minimal, the velocity above the internal umbrella-plate structure is considerably elevated. This indicates that in the region above the internal umbrella-plate structure, there is a considerable quantity of vapor-liquid mixed phase accumulation. The liquid phase is unable to flow smoothly out of the hole into the subsequent layer of the umbrella-plate structure. It is therefore inevitable that it will fall directly to the bottom of the liquid space, which will prevent the flash process from occurring. When the equilibrium constant *E* is equal to 9/184 and 3/46, the vapor-liquid velocity is approximately 2 m/s. This indicates that the velocity distribution of the mixed phase in the chamber is more uniform, which suggests that the liquid phase has flowed from the upper umbrella-plate layer into the lower layer and has been fully evaporated. This process has resulted in the formation of an obvious reflux phenomenon, which can promote heat and mass transfer in the chamber and strengthen the flash evaporation.

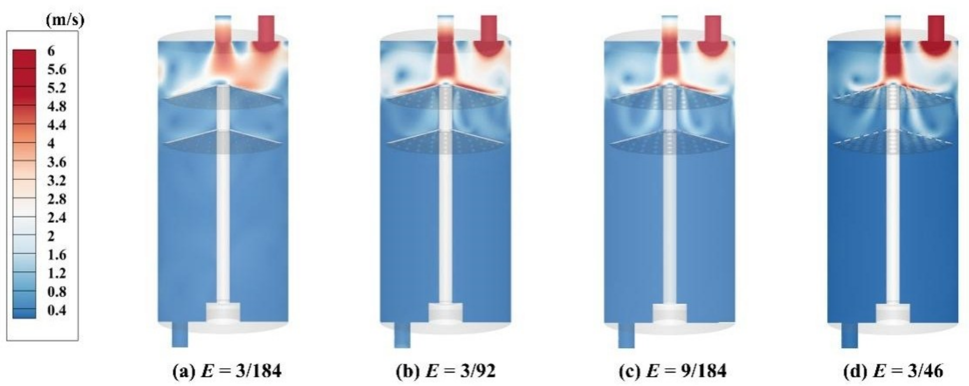

Figure 13 Velocity cloud maps at different aperture ratios *E*

Fig. 14 illustrates the temperature distribution within the chamber for both the multiple cut-offs reinforced internal components and the center section. The velocity cloud pattern is analogous to that observed in the previous case. When *E* is smaller, it can be observed that the temperature of the first umbrella-plate structure and the upper part is higher. This indicates that the liquid and the vapor-liquid mixture generated after flash evaporation accumulates in the umbrella-plate and the space above. When $E = 3/46$, the temperature distribution within the chamber is more uniform, and is approximately 325 K. This is accompanied by a more uniform temperature profile across the two umbrella-plate layers. The upper layer of liquid can flow smoothly to the lower layer, which can form droplets and spread into a liquid film, increasing the surface area exposed to the flash evaporation environment.

From Fig. 15 it can be seen that the average vacuum pressure in the chamber increases as *E* increases, which is not good for the flash evaporation process. However, from the flash evaporation rate results, the positive effect of the extended residence time of the liquid in the vapor space and the formation of behaviors such as droplets and liquid films outweighs the negative effect of the increase in the average vacuum pressure in the chamber, and a high degree of flash

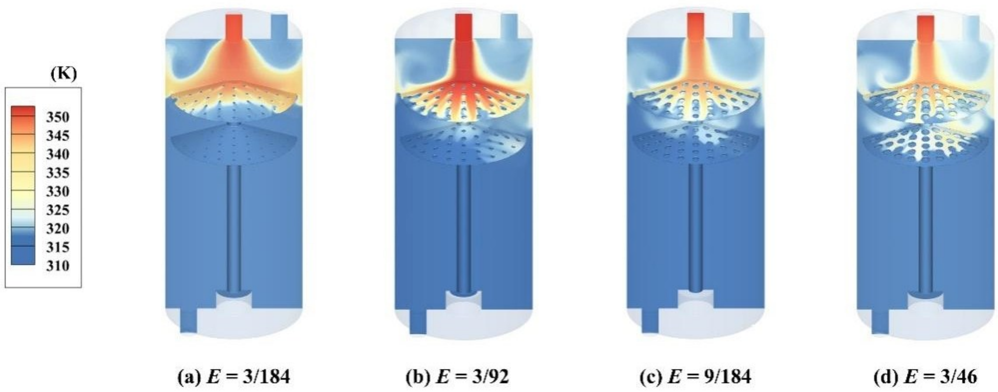

Figure 14 Temperature cloud maps in chamber at different aperture ratios E

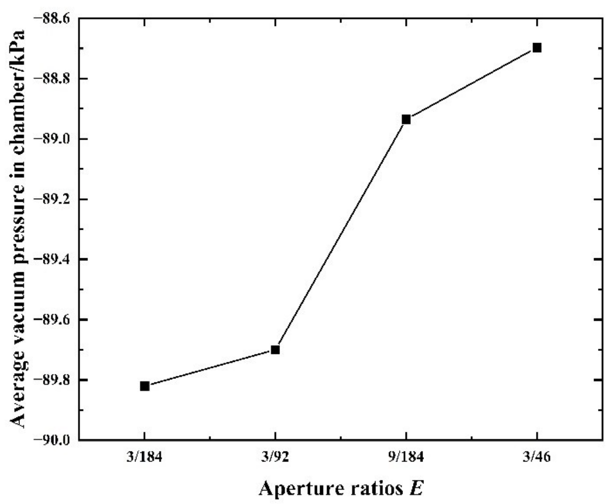

Figure 15 Average vacuum pressure in chamber for different aperture ratios E

evaporation completion is obtained when the liquid enters the chamber. Therefore, a higher value of E helps to improve the completion of the flash evaporation process.

6 Conclusions

A series of numerical simulations were conducted with the objective of investigating the impact of multiple intercepting and reinforcing structures on the flash evaporation characteristics. The effects of structural parameters, including the top angle, the aperture ratio, and the number of layers, on the flash evaporation process were the primary focus of this investigation. Upon analysis of the simulation results, the following conclusions can be drawn when the working conditions are certain.

(1) With the increase of the top angle θ of the internal component, it will slow down the falling speed of the liquid that is not completely flashed. When θ = 150°, the speed on the surface of first umbrella-plate structure layer is higher than 3.6m/s, and the speed on the surface of the second layer is higher than 1.6m/s. There is an obvious reflux formation, the growth rate of the flash evaporation rate is 81.91% compared to θ = 90°.

(2) With the increase of the number of layers N, it can prolong the time that the liquid stays in the flash vaporization environment, which is conducive to the completion of the whole flash vaporization process. When N = 5 can increase the flash evaporation rate by 17.51% compared with that of N = 2.

(3) With the increase of aperture ratio E, it is useful for the liquid on the upper layer to flow smoothly to the next layer. The incompletely flashed liquid can form into droplets and spread into liquid film. And it increases more surface area exposed to the flash environment. It produces an enhanced effect is greater than the negative impact of the increase in the average vacuum pressure inside the chamber. The flash evaporation rate at E = 3/46 is elevated by 100.84% compared to E = 3/184, which has a greater impact on the completion of the flash evaporation process.

About the Author

Wanqiong Bao, Graduated from Merchant Marine College of Shanghai Maritime University in 2021.Currently studying at School of Mechanical and Power Engineering, East China University of Science and Technology. Her research interests are in process intensification.

References

[1] Zhao Z H, Yuan Y C, Chen Yu, Meng F M, et al. Current state of research on flash evaporation characteristics and application of flash evaporation technology[J]. Energy and Environment, 2018(03): 25-27.

[2] Cai B, Yin Y, Zheng Y, et al. Mathematical study of spray flash evaporation in a spray-assisted seawater desalination chamber[J]. Desalination, 2019, 465 25-37.

[3] Stengler J, Schaber K, Mall-gleissle S, et al. Experimental study on low temperature desalination by flash evaporation in a novel compact chamber design[J]. Desalination, 2018, 448 103-112.

[4] Lee J G, Kim Y D, Kim W S, et al. Performance modeling of direct contact membrane distillation (DCMD) seawater desalination process using a commercial composite membrane[J]. Journal of Membrane Science, 2015, 478 85-95.

[5] Zhang K, Liu Z, Wang Y, et al. Flash evaporation and thermal vapor compression aided energy saving CO2 capture systems in coal-fired power plant[J]. Energy, 2014, 66 556-568.

[6] Yu X. J, Gao X, Zhong J. M. Simulation dynamics of the steam-powered catapult[J]. Ship & Ocean Engineering, 2005, 3: 1-4.

[7] Woods A, Bloom F, Orloff D. Modeling of flash evaporation Ⅰ: Formulation of the mathematical model[J]. Mathematical and Computer Modeling, 2000, 32(10): 1153-1169.

[8] Aoki I. Analysis of characteristics of water flash evaporation underflow-pressure conditions[J]. Heat Transfer Asian Research, 2000, 29(1): 22-23.

[9] Sebastian P, Nadeau J. Experiments and modeling of falling jet flash evaporators for vintage treatment[J]. International Journal of thermal sciences, 2002, 41: 269-280.

[10] Portha J F, Falk L, Commenge J M. Local and global process intensificated[J]. Chemical Engineering & Processing Process Intensificated, 2014, (84): 1-13.

[11] Sitter S, Chen Q, Grossmann I E. An overview of process intensificated methods[J]. Current Opinion in Chemical Engineering, 2019, (25): 87-94.

[12] Stefan Haase, Pasi Tolvanen, Vincenzo Russo. Process Intensification in Chemical Reaction Engineering[J]. Process, 2022, 10(1), 99.

[13] Sun Hong Wei, Chen Jian Feng. Advances in fundamental study and application of chemical process intensification technology in China[J]. Chemical Industry and Engineering Progress, 2011, 30(01): 1-15.

[14] Chen C, Zhang C. Numerical Simulation of Evaporation Characteristics of Flash Evaporation of Hot Water[J]. Power System Engineering, 2020, 36(05): 25-28.

[15] Pang Hong, Yao Zheng. Numerical modeling of flowing in the seawater desalting devices and its optimization[J]. Journal of Geological Hazards and Environment Preservation, 2004, (01): 37-41.

[16] Yao Zheng, Guo Chun. A study on the design of the flash chambers in multi-stage flash desalination devices[J]. Chinese Journal of Hydrodynamics, 2003, (04): 397-402.

[17] Qi Chun Hua, Fan Ming Ming, et al. Numerical Simulation of Flash Evaporation Characteristics and Optimization Design of Flash Tank for Seawater Desalination, 2009, 25(12): 87-91.

[18] Cao Tian Yi, Song Liang Fu. The Design of the Porous Plate in Flash Chamber of Multi-stage Sea Water Desalination Device[J]. Journal of Northeast Electric Power University, 2018, 38(06): 42-47.

[19] Seul K W, Lee S Y, Effect of liquid level on flow behaviour inside a multi-stage flash evaporator – a numerical prediction[J]. Desalination, 1992, 85: 161-177.

[20] Khamis Mansour M, Fath H E S. Numerical simulation of flashing process in MSF flash chamber[J]. Desalination and Water Treatment, 2013, 51 (10-12): 2231-2243.

[21] Zhang Rong Qing. Numerical simulation study of gas-liquid two-phase flow in bubbling carbonization tower [D]. Northeast Petroleum University, 2023.

[22] Wróbel K M. Modelling and numerical simulation of flows with evaporation and condensation[J]. 2005.

[23] Mansour A, Müller N. A review of flash evaporation phenomena and resulting shock waves[J]. Experimental thermal and fluid science, 2019, 107: 146-168.

[24] Darawsheh I, Islam M D, Banat F. Experimental characterization of a solar powered MSF desalination process performance[J]. Thermal Science and Engineering Progress, 2019, 10: 154-162.